Methods

Materials

All samples were collected from borehole cores of three well drillings (QT-2, E-27 and L-34) in the Ordos Basin, Inner Mongolia, northern China (Extended Data Figs. 1, 2). Five samples of black mudstone were macerated using hydrochloric-hydrofluoric acid maceration technique to extract meso- and microfossils. Organic residues were sieved through nylon mesh with 10 and 180 μm mesh openings, respectively, to eliminate impurities. Sample preparations were conducted in the Experimental Technologies Center of Nanjing Institute of Geology and Palaeontology (NIGP), Chinese Academy of Sciences (CAS). All original cores are deposited in the Exploration Department of PetroChina Changqing Oilfield Company, Xi'an, China. All prepared materials, including those of or in the form of rocks, residues, thin-section, and SEM stub, are deposited in the NIGP, CAS, with serial numbers and prefix PB.

Microscopies

Organic residues sieved on nylon mesh (10 μm mesh openings) were mounted onto glass slides with permount mounting medium. Slides were examined Under Zeiss Axio Imager.Z2 transmitted light microscope, and microfossils were photographed with AxioCam HRc digital camera. Mesofossils were initially examined under a binocular stereo microscope with incident light, and selected specimens were imaged using the Tescan MAIA3 scanning electron microscope. Morphologically valuable specimens were picked out, and then mounted on the inner wall of a slim tube to implement X-ray micro-tomography by the Zeiss Xradia 520 Versa tomographic microscope. Raw tomography data were processed by the software VGStudio Max 3.0 for three-dimensional reconstructions and virtual slices. All raw data are stored in the Big Data Center of the NIGP, CAS.

Geological age

Geological ages of our samples are determined by marine fossils and bio-stratigraphical correlation.

The borehole QT-2 core (well depth 4658-4659 m, round 6-17/30) yields stomata and posable tracheid fragments, marine fossils from this bed include: chitinozoans (*Belonechitina cactacea brevis*, *B*. *hirsute*, *Cyathochitina cycnea*, *C*. *hunderumensis*, *Desmochitina minor* group, *Lagenochitina pirum*) and graptolites (*Cryptograptus tricornis*, *Dicranograptus* sp. indet, ?*Jiangxigrpatus intortus*, *Pseudazygograptus incurvus*).

The borehole E-27 core (well depth 3959-3962 m, rounds 7-7/46, 7-14/46 and 7-17/46) consists of much mudstone with plenty of plant debris. Three samples from this portion were macerated and we obtain plant fragments of branched axis with or without tracheids, and stoma. One limestone sample overlaying the mesofossil-bearing beds contains conodonts *Drepanodus* sp., and the lower limestone contains conodonts *Protopanderodus cooperi*, *Periodon* sp., and *Pygodus* sp. The sample E-27(7-7/46) contains chitinozoans *Conochitina ordinaria* and *Lagenochitina pirum*, and the sample E-27(7-17/46) contains chitinozoans *Belonechitina cactacea brevis*, and *B*. cf. *henryi*.

The borehole L-34 core (well depth 3954-3956 m) consists of mudstone and yields mesofossils of tracheid, and also chitinozoans *Belonechitina cactacea typica*, *Kalochitina brevispinosa*, *Lagenochitina* aff. *pirum*, *L*. sp. A, and *Sphaerochitina* cf. *gracqui*. The aforementioned marine fossils as a whole indicate a Darriwilian to Sandbian age, and the graptolites of *Nemagraptus gracilis* biozone constrain the age of fossil-bearing horizon to early Sandbian (Goldman et al., 2020).

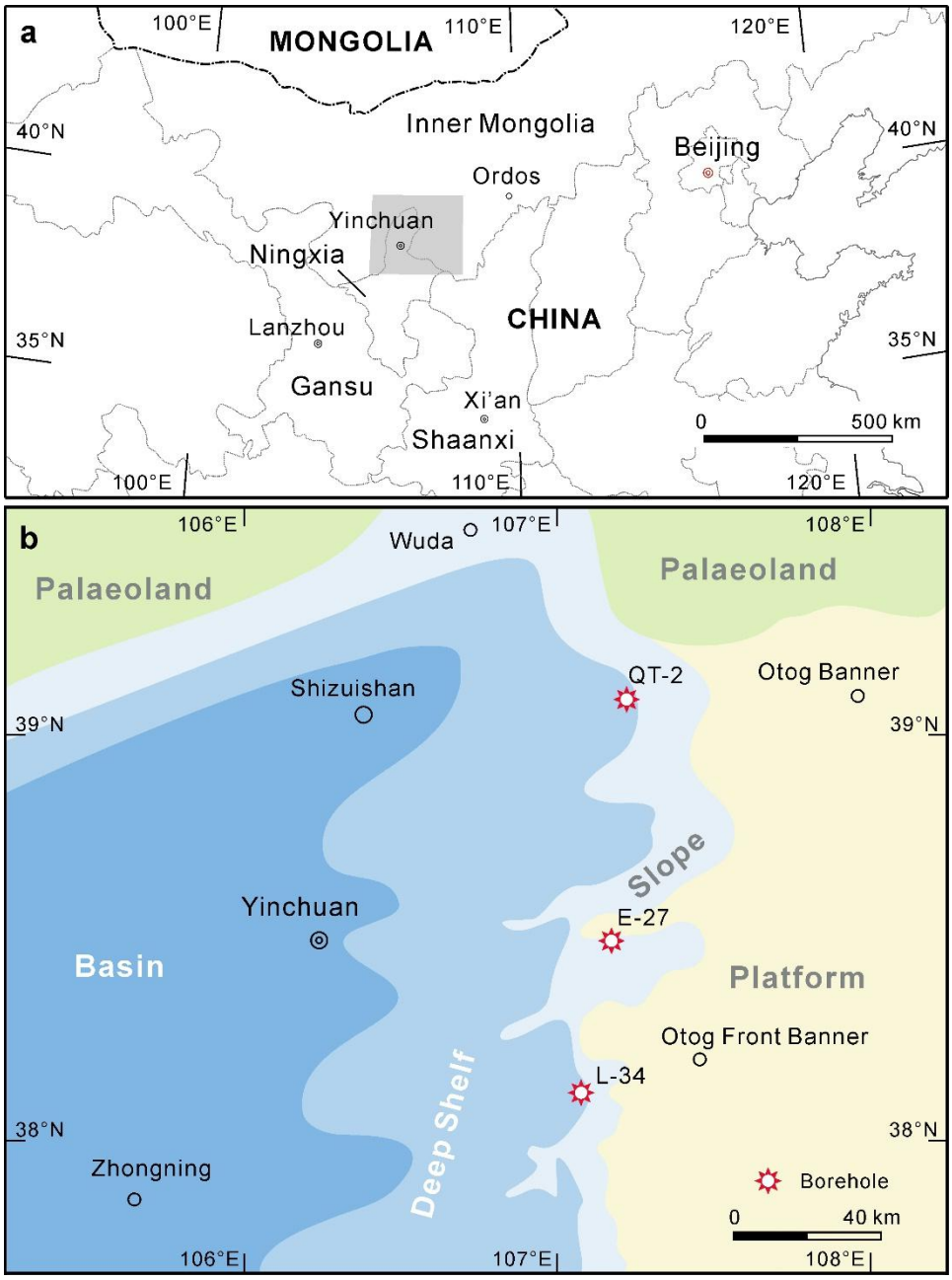

Extended Data Fig. 1 Geographic map and geologic setting of the fossil locality. a, Geographic map showing the location of the study area (marked by dark grey rectangle). **b**, Sedimentary facies of the study area during mid-late Ordovician (modified from Yu et al., 2021), noting all sampled boreholes are located in the slope area, fossil plant debris are probably derived from the flora dwelling in the nearshore area.

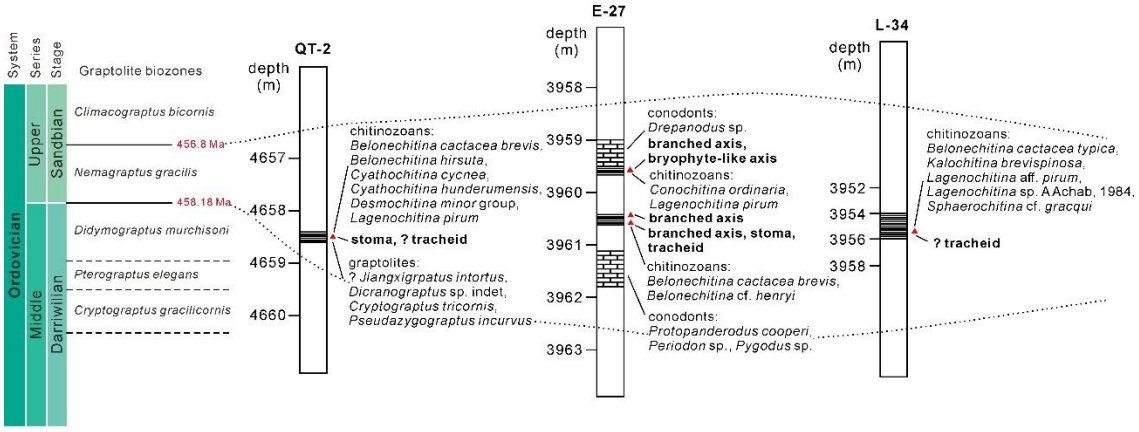

Extended Data Fig. 2 Stratigraphic position and fossils of the borehole cores. Graptolite biozones and numerical ages are based on Chen et al. (2016) and Goldman et al. (2020), respectively. Red triangles by columns refer to plant fossils-bearing beds.

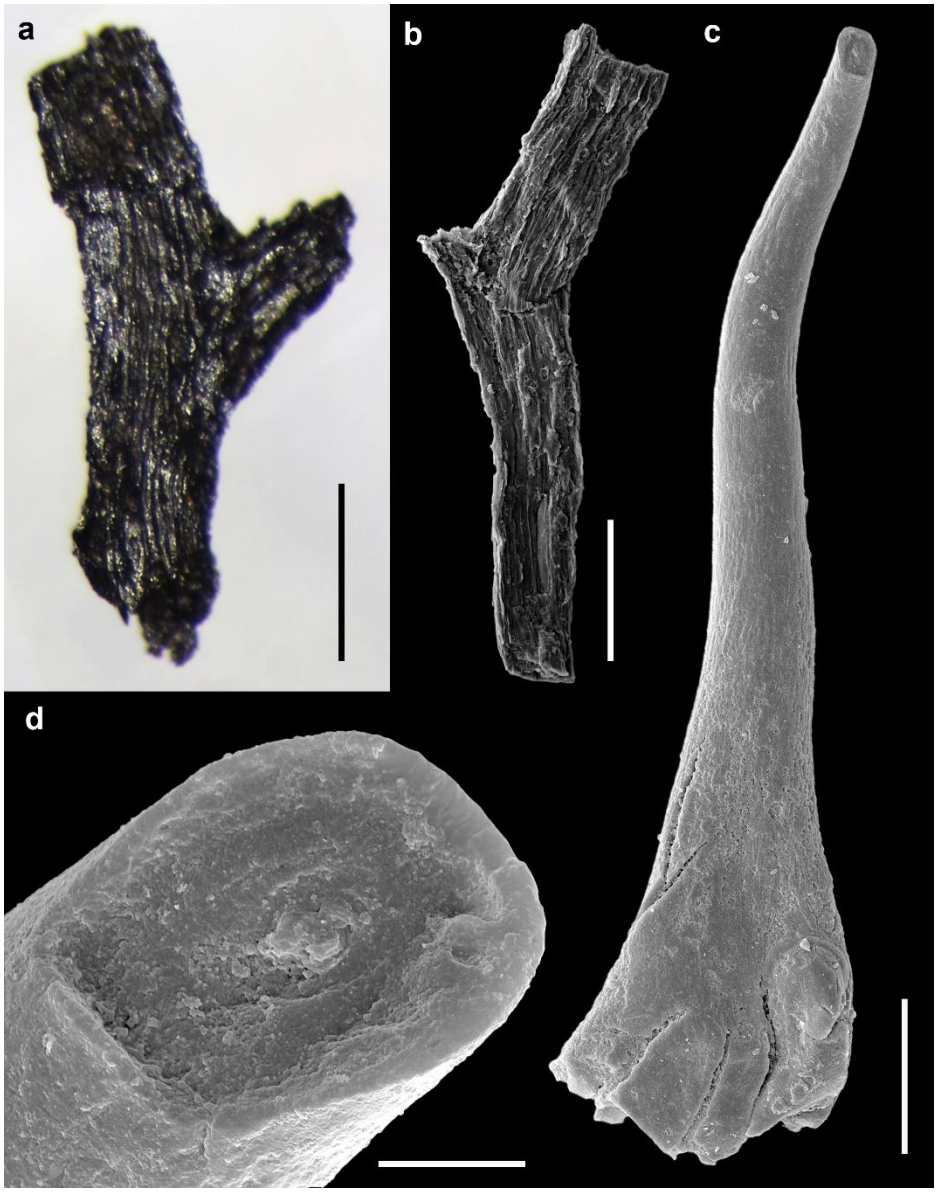

Extended Data Fig. 3 A dichotomously branched axes (a, b) and an isolated leaf-like structure (c, d) from the Upper Ordovician of China. a, Incident light microscopy photograph of the branched axis in Fig. 1a. **b**, Scanning electron microscopy photograph of a branched axis. Specimen from E-27 borehole (E-27, 7-17/46). PB24386. **c**, Scanning electron microscopy photograph of an isolated leaf-like structure. Specimen from E-27 borehole (E-27, 7-17/46). PB24430. **d**, Close-up of the oblique, transversely fractured surface of the distal end in **c**. Scale bars: 200 μm for **a**, **b**, **c**; 20 μm for **d**.

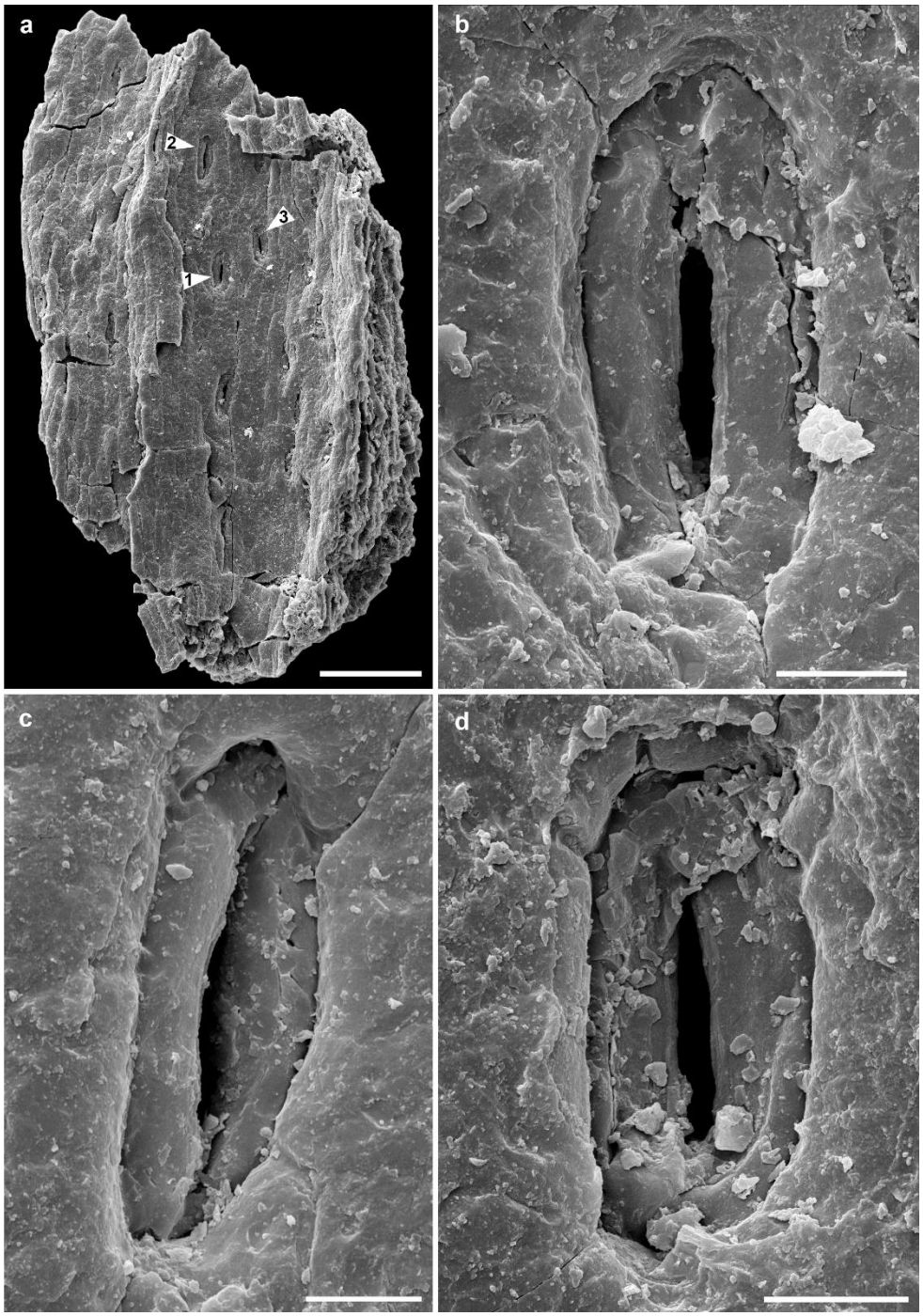

Extended Data Fig. 4 Additional epidermis fragment with stomata, from the Upper Ordovician of China. a, Scanning electron microscopy photograph of the intact specimen. **b**-**d**, Close-ups of the stomata indicated by arrows 2, 1, and 3 in **a** respectively. Stomata are clearly sunken. Specimen from E-27 borehole (E-27, 7-17/46). PB24402. Scale bars: 100 μm for **a**; 10 μm for **b**-**d**.

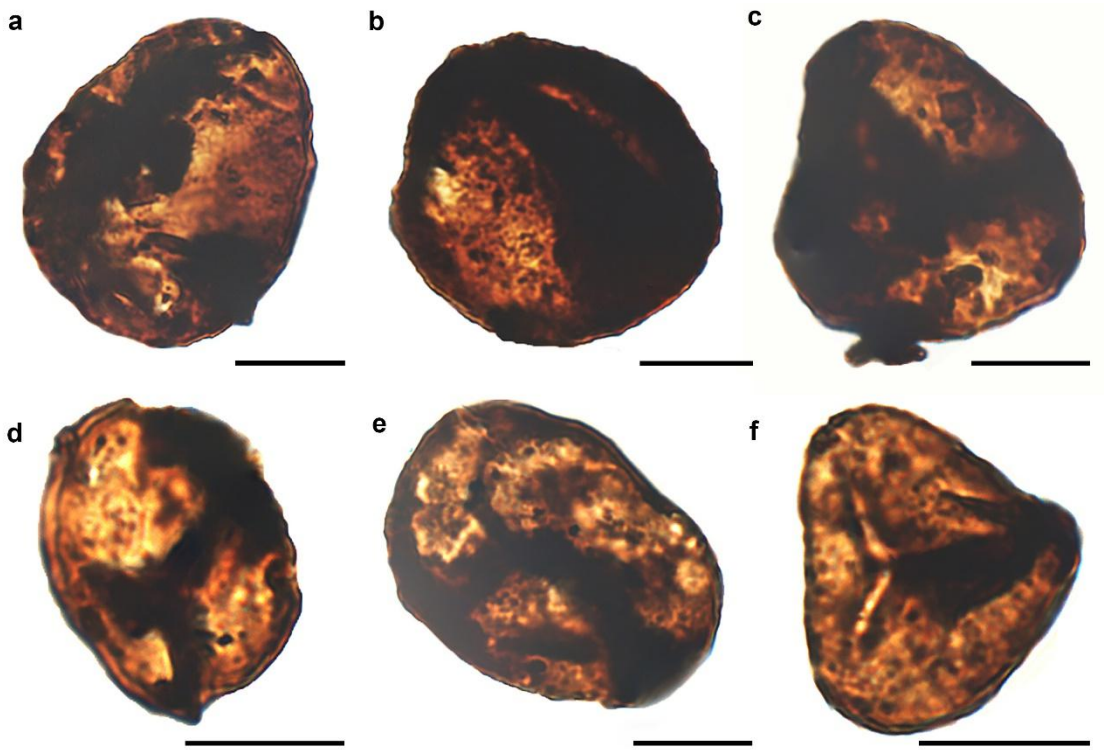

Extended Data Fig. 5 Trilete spores and cryptospores from the Upper Ordovician of China. All specimens from E-27 borehole (E-27, 7-17/46). **a**, Cryptospore monad. (99.7, 8) of PB24546. **b**, Cryptospore dyads similar to *Segestrespora rugosa*. (93, 10) of PB24545. **c-f**, Trilete spores. (91, 13.5) of PB24543, (98, 5) of PB24541, (88, 15) of PB24544, and (99.5, 8) of PB24540, respectively. Scale bar: 10 μm for all.

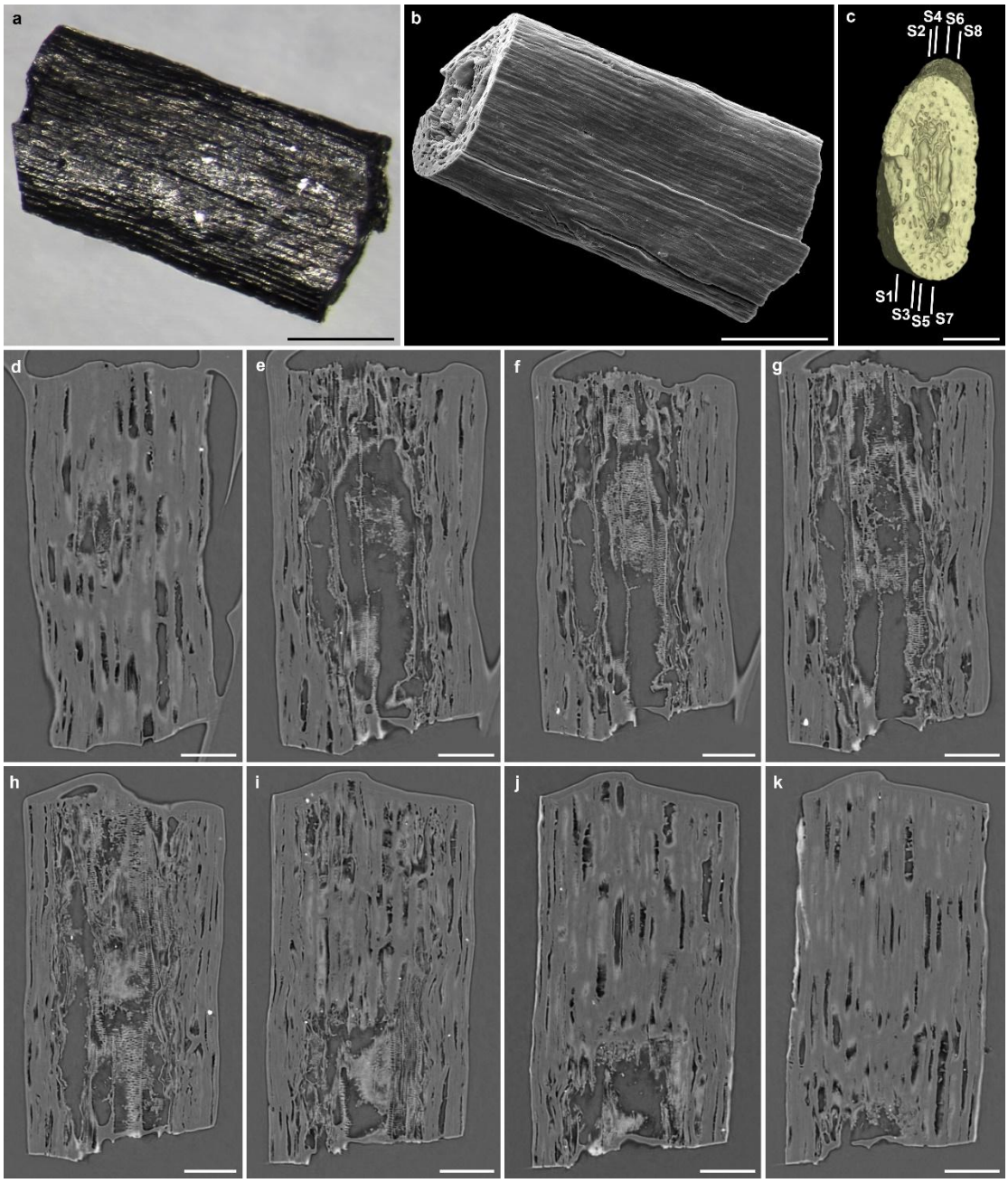

Extended Data Fig. 6 Additional images of the tracheid-bearing axis in Fig. 2. **a**, Incident light microscopy photograph of the axis. **b**, Scanning electron microscopy photograph of the axis. **c**, Transverse view of the axis, based on three-dimensional reconstruction. S1-S8 in **c** mark the locations of slice views in **d**-**k**, respectively. **d**-**k**, X-ray micro-tomography virtual slices, longitudinally viewed (perpendicular to the direction of compression). Scale bars: 200 μm for **a**,**b**; 100 μm for **c**-**k**.

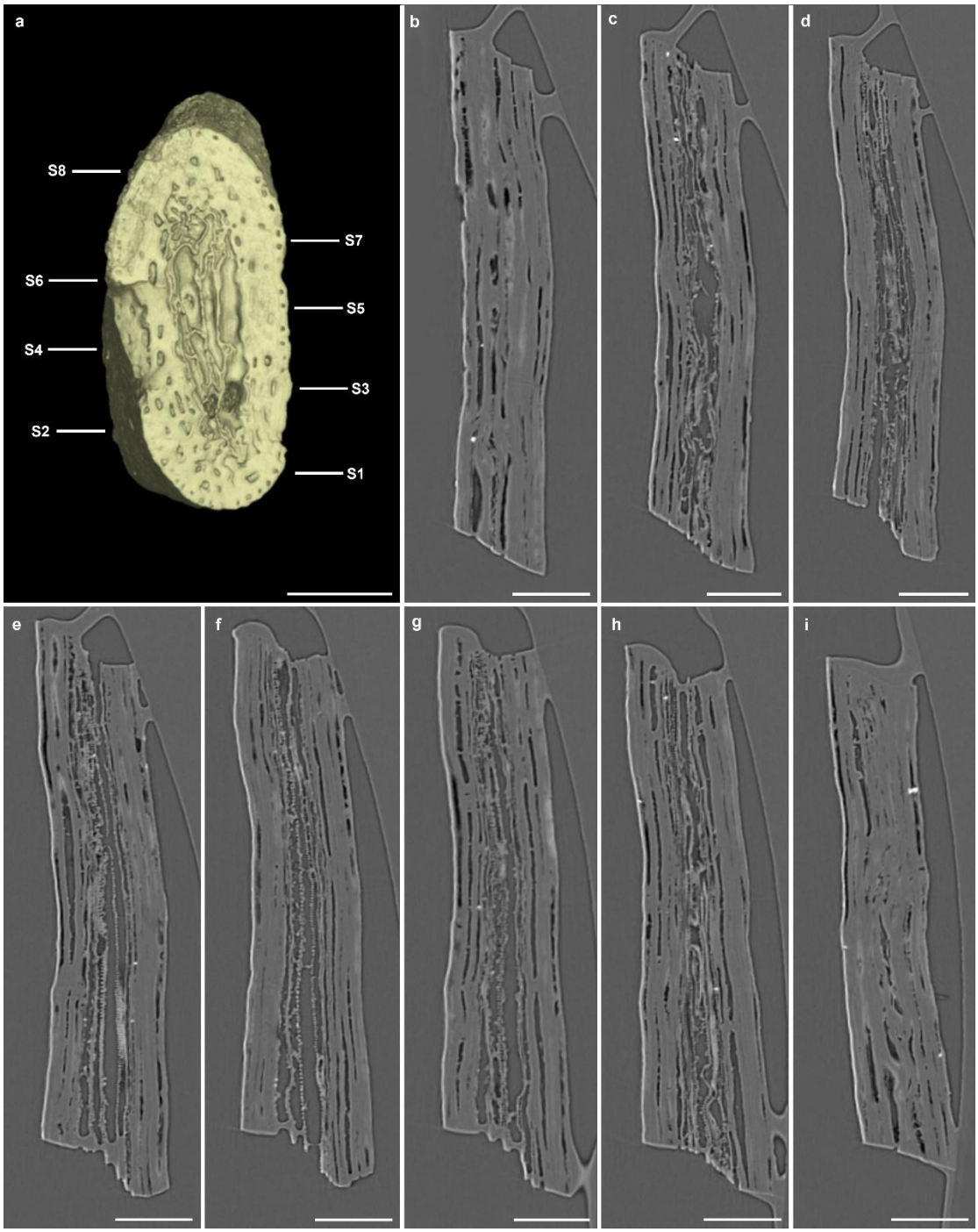

Extended Data Fig. 7 Additional images of the tracheid-bearing axis in Fig. 2. a, Transverse view of the axis, based on three-dimensional reconstruction. S1-S8 in **a** mark the locations of slice views in **b-i**, respectively. **b-i**, X-ray micro-tomography virtual slices, longitudinally viewed (parallel to the direction of compression). Scale bar: 100 μm for all.

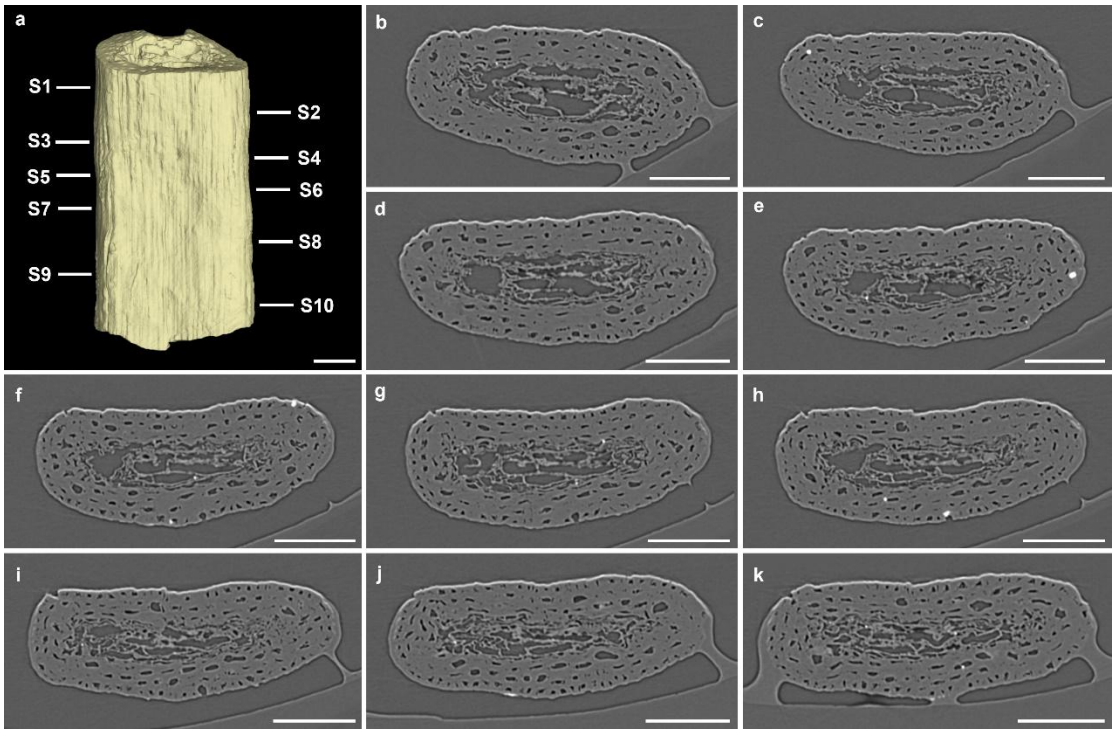

Extended Data Fig. 8 Additional images of the tracheid-bearing axis in Fig. 2. a, Longitudinal view of the axis, based on three-dimensional reconstruction. S1-S10 in **a** mark the locations of slice views in **b**-**k**, respectively. **b**-**k**, X-ray micro-tomography virtual slices, transversely viewed. Scale bar is 100 μm for all images.

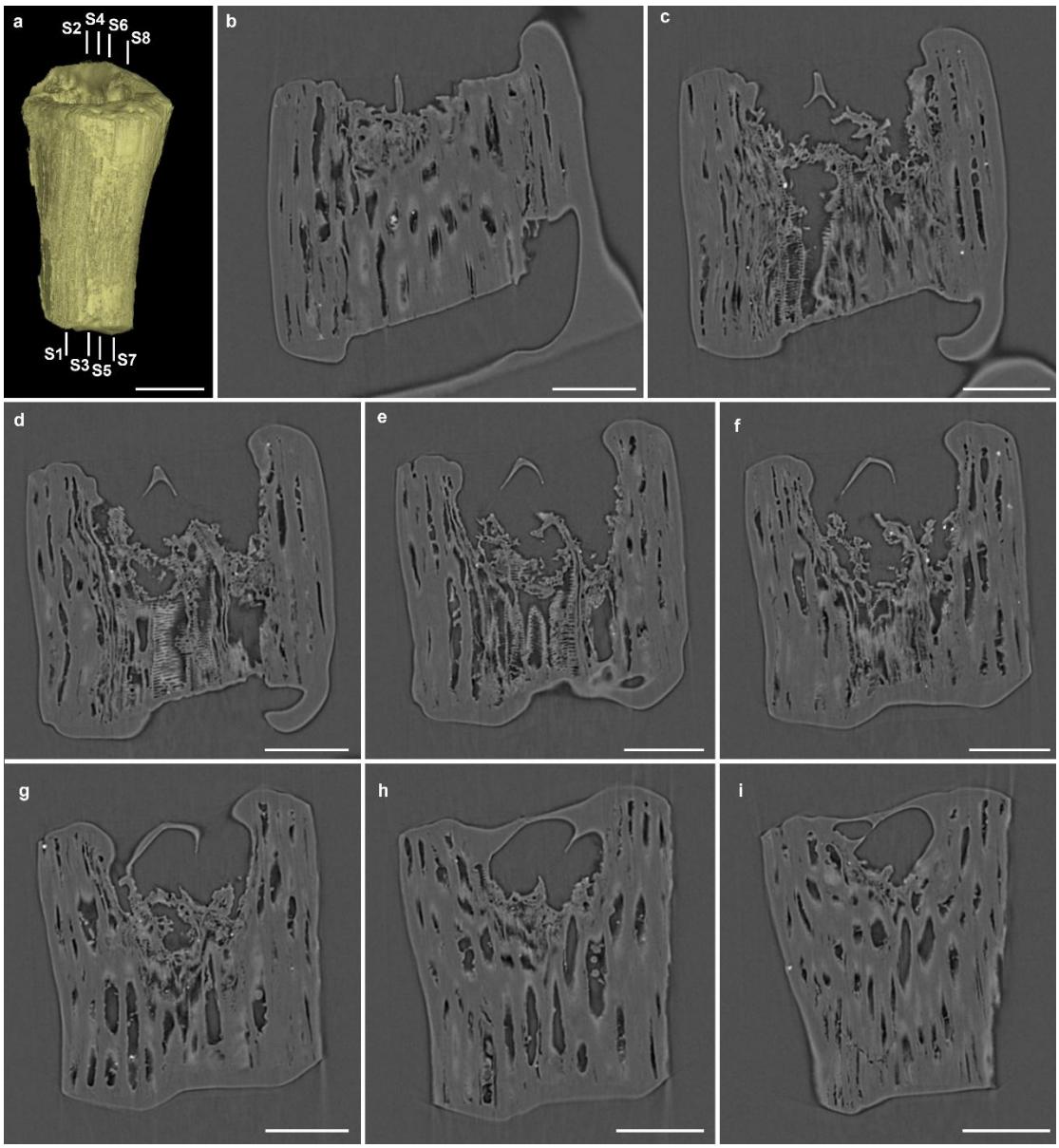

Extended Data Fig. 9 Another tracheid-bearing axis from the Upper Ordovician of China. a, Longitudinal view (perpendicular to the direction of compression) of the axis, based on three-dimensional reconstruction. S1-S8 in **a** mark the locations of slice views in **b-i**, respectively. **b-i**, X-ray micro-tomography virtual slices, longitudinally viewed. Specimen is from E-27 borehole core (E-27, 7-7/46). PB24428. Scale bar: 100 μm for all.

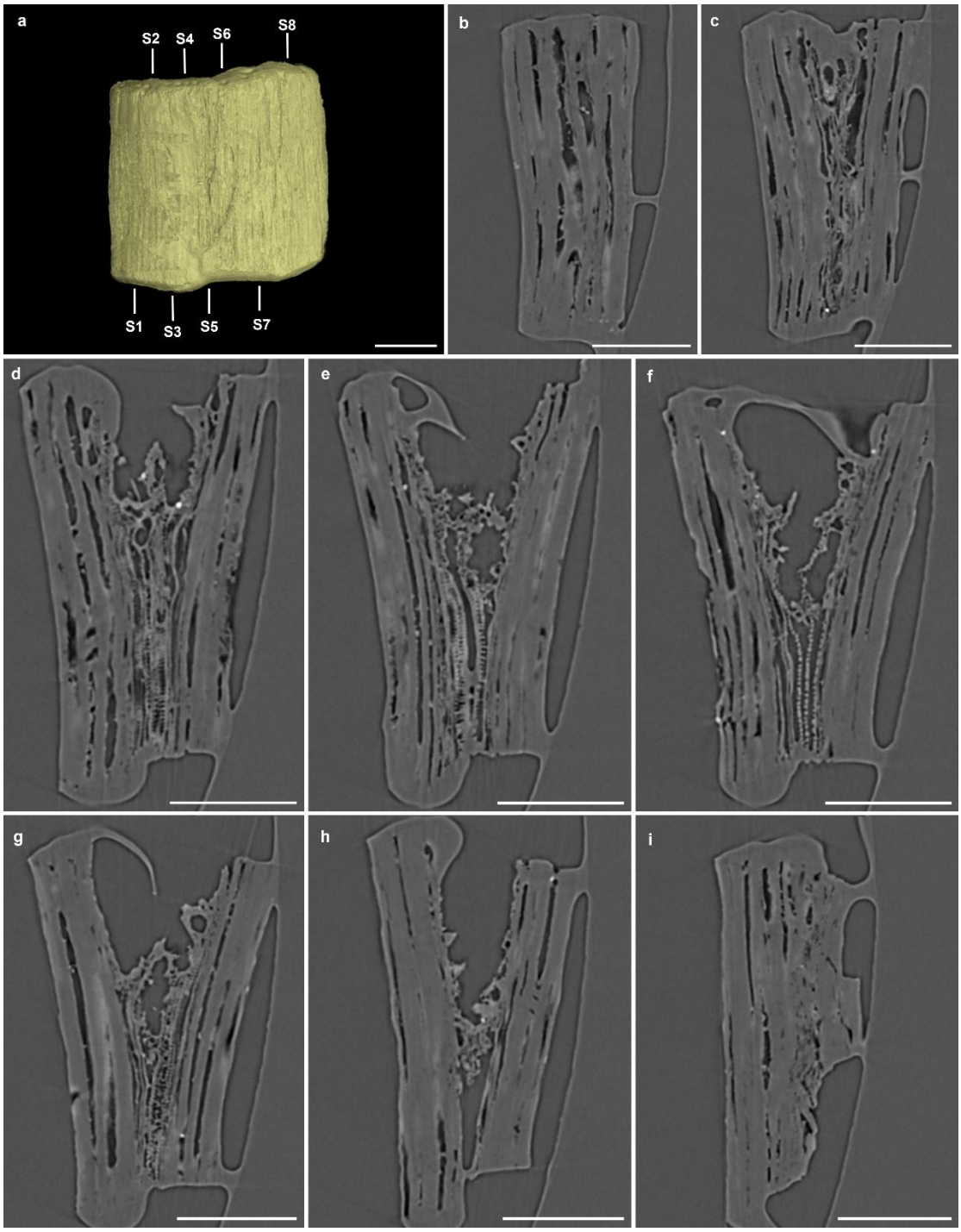

Extended Data Fig. 10 Additional images of the tracheid-bearing axis in Extended Data Fig. 9. a, Longitudinal view (parallel to the direction of compression) of the axis, based on three-dimensional reconstruction. S1-S8 in **a** mark the locations of slice views in **b-i**, respectively. **b-i**, X-ray micro-tomography virtual slices, longitudinally viewed. Scale bar: 100 μm for all.

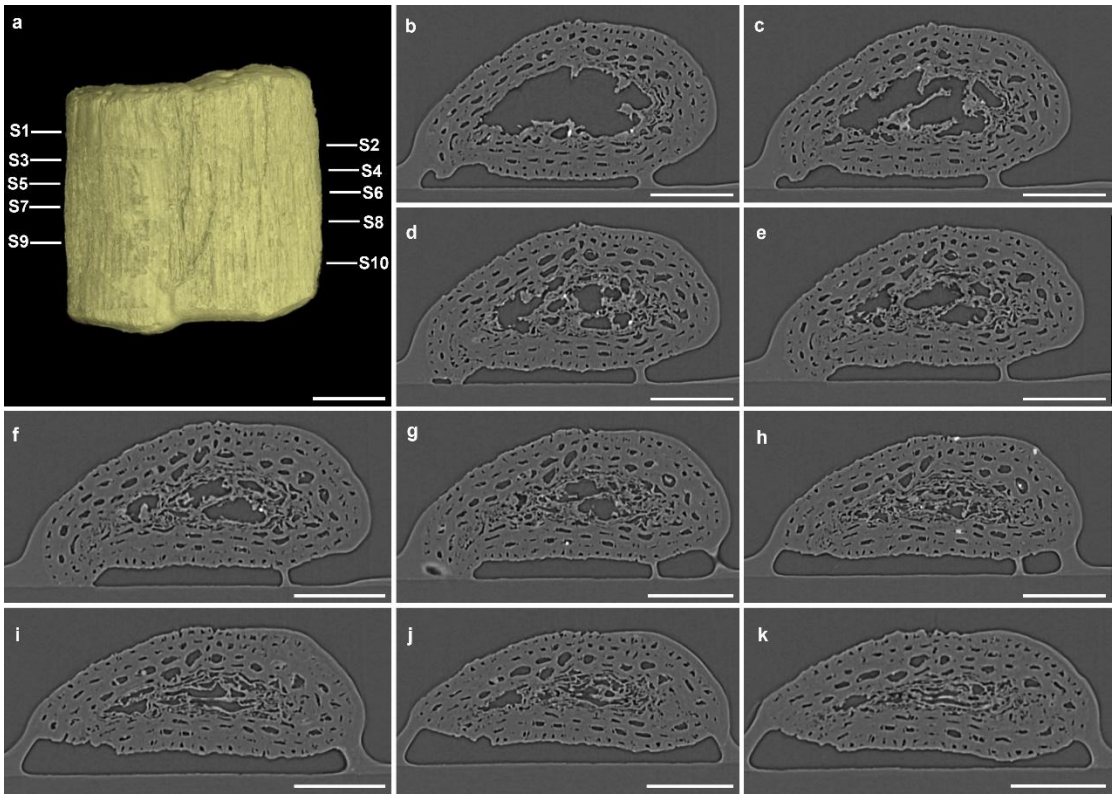

Extended Data Fig. 11 Additional images of the tracheid-bearing axis in Extended Data Fig. 9. a, Longitudinal view (parallel to the direction of compression) of the axis, based on three-dimensional reconstruction. S1-S10 in **a** mark the locations of slice views in **b**-**k**, respectively. **b**-**k**, X-ray micro-tomography virtual slices, transversely viewed. Scale bar: 100 μm for all.

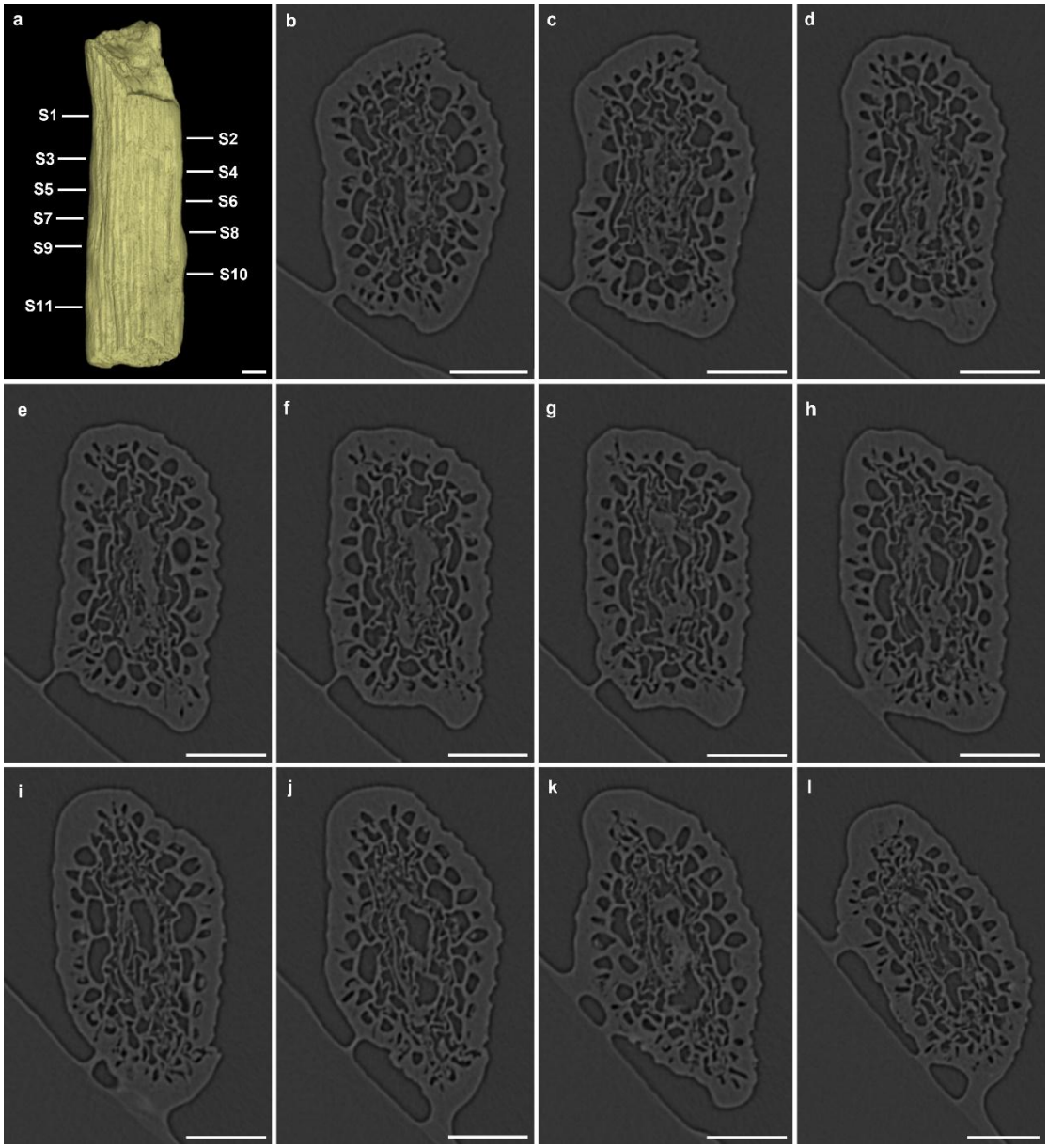

Extended Data Fig. 12 An unbranched axis with bryophyte-like stem structure, from the Upper Ordovician of China. a, Longitudinal view of the axis, based on three-dimensional reconstruction. S1-S11 in **a** mark the locations of slice views in **b-l**, respectively. Specimen from E-27 borehole (E-27, 7-7/46). PB24429. **b-l**, X-ray micro-tomography virtual slices, transversely viewed. Scale bar: 50 μm for all.

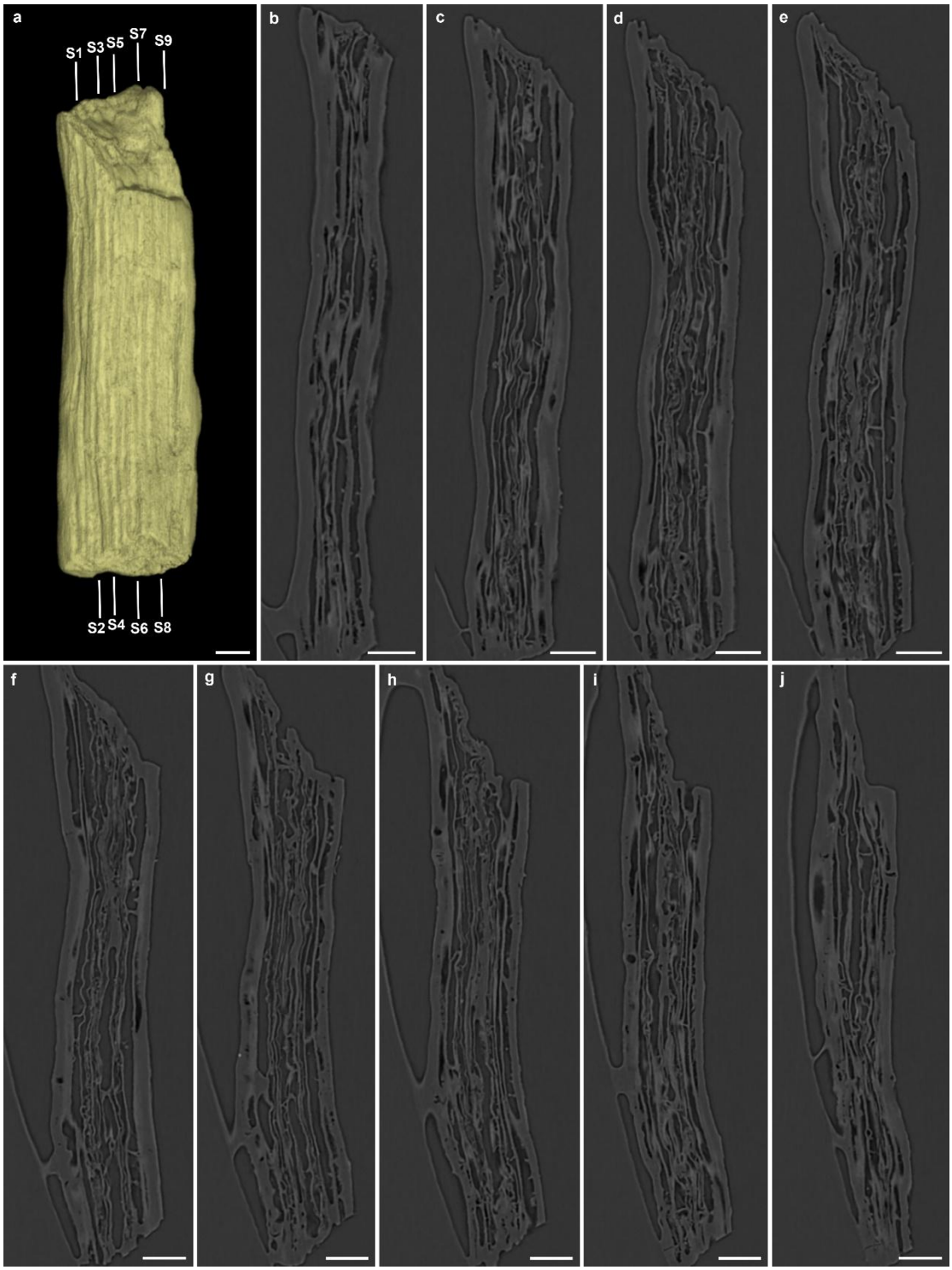

Extended Data Fig. 13 Additional images of the axis in Extended Data Fig. 12. a, Longitudinal view of the axis, based on three-dimensional reconstruction. S1-S9 in **a** mark the locations of slice views in **b-j**, respectively. **b-j**, X-ray micro-tomography virtual slices, longitudinally viewed. Scale bar: 50 μm for all.

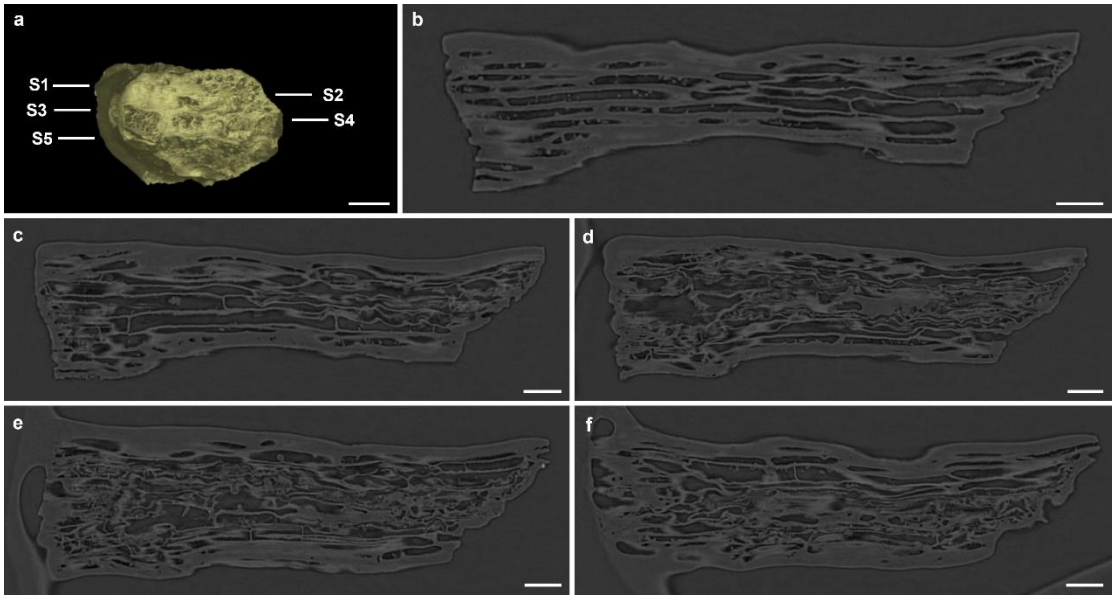

Extended Data Fig. 14 Additional images of the axis in Extended Data Fig. 12. a, Transverse view of the axis, based on three-dimensional reconstruction. S1-S5 in **a** mark the locations of slice views in **b**-**f**, respectively. **b**-**f**, X-ray micro-tomography virtual slices, longitudinally viewed (perpendicular to the direction of **b**-**j** in Extended Data Fig. 12). Scale bar: 50 μm for all.

Extended Data Tab. 1 Comparisons of water-conducting cell types in primitive land plants. Sw/Ss (%) refers the area percentage of water-conducting cells taking by the whole stem in traverse view. This ratio of *Cooksonia pertoni* is directly cited from Edwards et al., 1992, and those of other taxa are calculated based on specimens therein.

Taxon	Age	Strata and locality	Water-conducting cell type	Sw/Ss(%)	Reference
Tracheid-bearing axis	early Sandbian, Late Ordovician	E-27 borehole, Inner Mongolia, northern China	scalariform, reticulate (tracheids)	36.7	this text
Aglaophyton majus	Pragian to Emsian, Early Devonian	Rhynie cherts, Scotland	no secondary thickenings (similar to hydroids)	1.36	Kerp, 2017
Horneophyton lignieri (Horneophytes)	Pragian to Emsian, Early Devonian	Rhynie cherts, Scotland	narrow, irregular, annular and/or, spiral (tracheids)	—	Cascales-Miñana et al., 2019
Rhynia gwynne-vaughanii (Rhyniophytes)	Pragian to Emsian, Early Devonian	Rhynie cherts, Scotland	S-type (tracheids)	0.5	Kerp, 2017
Cooksonia pertoni	Lochkovian, Early	Lower Old Red	S-type (tracheids)	1.45 ~ 2.04	Edwards et al., 1992

	Devonian	Sandstone, England			
Asteroxylon mackiei (Lycophytes)	Pragian to Emsian, Early Devonian	Rhynie cherts, Scotland	G-type (tracheids)	1.42	Edwards, 1993
Haplomitrium hookeri (Liverworts)	extant	—	no secondary thickenings (hydroids)	1.46	Ligrone et al., 2000
Pogonatum aloides (Mosses)	extant	—	no secondary thickenings (hydroids)	1.76	Ligrone et al., 2000
Plagiomnium undulatum (Mosses)	extant	—	no secondary thickenings (hydroids)	4.76	Ligrone et al., 2000

168